Available online at www.sciencedirect.com
SCIENCE DIRECT®
International Journal of Heat and Mass Transfer 47 (2004) 4857–4867
International Journal of HEAT and MASS TRANSFER
www.elsevier.com/locate/ijhmt

Combustion of propanol–glycerol mixture droplets in reduced gravity

V. Dee, B.D. Shaw *

Mechanical and Aeronautical Engineering Department, University of California, Davis, CA 95616, USA

Received 6 June 2003; received in revised form 30 April 2004

Abstract

Reduced-gravity experiments on combustion of propanol–glycerol mixture droplets were performed. Droplets were initially about 1 mm in diameter with initial glycerol mass fractions of 0, 0.05 and 0.2. All experiments were in air at standard temperature and pressure. Experiments showed flame contractions, and data on burning rates and onset times for flame contraction allowed effective species diffusivities to be estimated. Comparison of the experiments with computational modeling suggests that convective mixing was likely present in the droplets. Propanol–glycerol droplets sometimes exhibited extinction after flame contraction. This behavior has been previously observed only for much larger droplets burned in space-based experiments.
© 2004 Elsevier Ltd. All rights reserved.

1. Introduction

The evaporation and combustion characteristics of fuel droplets have been the subject of numerous investigations because of their relevance to the efficient use of fuel sprays as well as for scientific reasons. In an effort to provide data that can be compared with simplified analytical and computational models, many investigations have focused on studying evaporation and combustion of fuel droplets under conditions where buoyancy effects are negligible. In addition, it is of interest to investigate combustion behaviors of multicomponent droplets because practical fuels are multicomponent in nature. This research focuses on combustion behaviors of what are arguably the simplest miscible mixtures, namely, binary fuel droplets. Reduced gravity is employed in the experiments to strongly promote spherical symmetry in the gas phase, allowing comparison with theoretical models that neglect buoyancy effects.

The droplets used in the present research were composed of mixtures of 1-propanol (denoted as propanol) and glycerol, with initial liquid glycerol mass fractions, Y, of 0 (pure propanol), 0.05 and 0.20. All experiments were conducted in air at 0.1 MPa and about 298 K, and droplets were initially about 1 mm in diameter. In addition, asymptotic theory and computational modeling have been employed to aid interpretation of the experimental results. The initial glycerol mass fractions used in the experiments were selected so that influences of the initial glycerol loading could be investigated. These particular values of Y were selected because they were expected to lead to significant differences in droplet and flame size histories.

Propanol/glycerol mixtures were investigated in the present experiments because these mixtures have physical properties that are useful for scientific studies. For example, propanol and glycerol have widely different boiling points (the boiling points of propanol and glycerol at 1 atm are 370 and 563 K, respectively), which leads to so-called sudden flame contractions. Flame contractions are caused by rapid droplet heating [1,2], which occurs as the mass fraction of the low-volatility component (glycerol) near the droplet surface approaches unity. The onset time for flame contraction can

* Corresponding author. Tel.: +1-530-752-4130; fax: +1-530-752-4158.
E-mail address: bdshaw@ucdavis.edu (B.D. Shaw).

0017-9310/$ - see front matter © 2004 Elsevier Ltd. All rights reserved.
doi:10.1016/j.ijheatmasstransfer.2004.05.025

Nomenclature

a_1	coefficient in Eq. (13)
a_2	coefficient in Eq. (13)
c	liquid-phase specific heat
d	droplet diameter
D	liquid-phase species diffusivity
E	liquid transport enhancement factor
g_0	normal gravitational acceleration (9.81 m/s^2)
i	grid point
L	enthalpy of vaporization
$\dot{m}$	mass flow rate off the droplet surface
N	number of grid points
Pe	Peclet number (Ud/D_{char})
R	radius of droplet
$\dot{R}$	$\mathrm{d}R/\mathrm{d}t$
r	radial coordinate
T	temperature
t	time
U	characteristic liquid velocity
V	liquid diffusion velocity
v	bulk velocity in the liquid phase
Y, y	mass fraction
z	dimensionless radial coordinate

Greek symbols

β	grid spacing parameter
δ	mass flux fraction of glycerol from the droplet surface
λ	liquid thermal conductivity
ρ	liquid density
ϕ	variable in Eq. (13)
ν	characteristic liquid kinematic viscosity

Subscripts

a	glycerol
act	actual
b	propanol
char	characteristic
+	gas side of the gas–liquid interface
−	liquid side of the gas–liquid interface

Superscript

∘	infinitely-dilute solution

be used to estimate effective liquid species diffusivities of mixture droplets [2,3]. The term "effective diffusivity" refers to the diffusivity that is required in a spherically symmetrical (convection free) configuration to reproduce experiments that actually involve liquid convection. In other words, effective diffusivity is the diffusivity enhanced by convection. It is noted that glycerol has a much higher surface tension than propanol, which could potentially lead to droplet interior flows driven by Marangoni effects [4]. Glycerol is also more viscous than many liquid fuels, which can influence convective mixing rates inside droplets by reducing liquid convective flow velocities. It is also mentioned that while propanol/glycerol mixtures were investigated here for particular scientific reasons, combustion of droplets containing propanol is of interest in itself since propanol is an alcohol and alcohols have been considered as alternative fuels.

A goal of the research was to investigate whether mixing was occurring in the droplets. Droplet internal mixing could potentially be driven by factors such as droplet formation and deployment mechanisms or perhaps Marangoni instabilities. This goal was pursued by comparing the experimental results on flame contraction to theoretical results predicting flame contraction, where the theory neglects interior liquid flows. Ideally, it is desirable to obtain information on the character of droplet internal flows because the internal flowfield can appreciably influence the effective species diffusivity. However, visualization of flows inside droplets that are burning in a microgravity environment is difficult, and this difficulty extended to the present experiments. Instead, experimental data on flame contraction were compared with theoretical models that assume that convective flows in the liquid are negligible. In this way, inferences can be made on whether significant convective flows, which increase species transport rates, were present in the droplets.

The importance of convective flows on species transport in the liquid phase can be estimated by noting the magnitude of the liquid phase Peclet number (Pe). Defined as $Pe = Ud/D_{\text{char}}$, the Peclet number is a ratio of characteristic times for species transport from convection and diffusion, respectively. The velocity U represents a characteristic droplet interior velocity, e.g., from circulatory flows induced by external convection (surface shear stresses) or Marangoni stresses. This velocity may be determined by solving the equations for conservation of momentum and mass inside the droplet subject to appropriate conditions at the liquid–gas interface. In the limit of very slow internal flows ($Pe \ll 1$), convective effects are small and the characteristic length scale for species diffusion is the droplet radius. If a Hills-type vortex is present in a droplet ($Pe \to \infty$), effective species diffusivities can be larger than molecular diffusivities by a factor of up to about 2.7 [5]. In this case, contours of constant composition closely follow streamlines, and diffusive length scales are

reduced to essentially the distance between the vortex center and the droplet surface. However, if chaotic flows are present in droplets, effective species diffusivities can be even larger [6] (for $Pe \gg 1$) because of decreases in diffusive length scales within droplets.

The results in this paper represent the first data on reduced-gravity combustion of bi-component droplets composed of propanol–glycerol mixtures. It is noted, however, that other bi-component mixture droplets have been studied in reduced-gravity combustion environments. For example, heptane–hexadecane, methanol–dodecanol, ethanol–dodecanol, methanol–water, ethanol–water, and heptane–monochloroalkane droplets have been studied using ground-based and space-based facilities [3,7–13]. Depending on the compositions of the liquid and gas phases as well as the environmental pressure, wide variations in combustion phenomena such as liquid mixing rates, soot formation, and extinction have been demonstrated. A review of results obtained from reduced-gravity droplet combustion investigations is available [14].

2. Experimental apparatus and test procedures

Experiments were conducted at the 2.2 s drop tower at the NASA Glenn Research Center at Lewis Field in Cleveland, Ohio [15]. This drop tower provides gravity levels about $10^{-4}g_0$. NASA provided the experiment rig used in the tests. The rig weighed about 300 pounds and contained a sealed test chamber, four battery packs, two video cameras, and control electronics.

The sealed chamber contained two deployment needles, one of which was connected to a syringe via a small plastic tube. A stepper motor controlled dispensing of fuel from the syringe to the needle. Two independent servomotors were used to rotate the dispensing needles, and two other stepper motors independently positioned the hot-wire ignition elements. A 15 μm silicon carbide fiber placed between two brass posts was located symmetrically between the needles and the hot-wire ignition elements. The fiber was used to prevent excessive droplet drift during the experiments. A schematic of the droplet dispensing and ignition assembly is shown in Fig. 1.

During the pretest setup, the test rig was enclosed in a drag shield and raised to the top of the drop tower. At the top of the tower, a hand-held control box was connected via serial cable to the drop rig controls to set the experiment. The flame view camera was turned on and the image inside the test chamber was displayed on the monitor next to the recording equipment in order to perform the setup. The dispense needles were retracted to home position and then moved one at a time until they came in contact with the support fiber. Moving the needles was performed in multiple steps in order not to damage them. Fuel was dispensed in normal gravity just

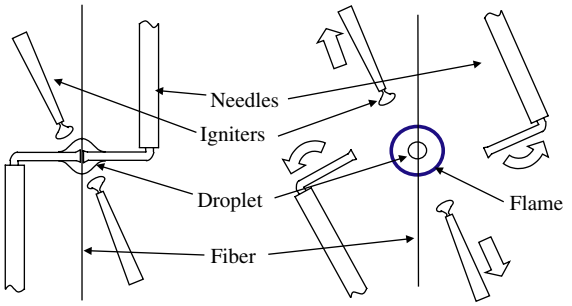

Fig. 1. Droplet before and after ignition.

prior to the start of a test. A stepper motor dispensed a droplet approximately 1 mm in diameter onto the fiber. Once the droplet was on the fiber, the deployment needles were slowly retracted until the flared tip barely made contact with the edge of the droplet, stretching it to facilitate better deployment. Next, the igniter elements were moved to within 5 mm of the droplet. Similar to positioning of the needles, igniters were moved in a single motion until they were visible on the setup monitor and then in small steps towards the droplet. At this point, the package was released into free fall and the needles were rapidly retracted, leaving the droplet on the fiber. The hot wire igniters were then briefly heated with a controlled current, igniting the droplet, and then retracted away from the droplet and the flame. Ignition was set to occur 100 ms after release and each igniter wire dissipated about 3.5 W for 250 ms. The droplet burned until either the fuel was spent, the drop rig hit the air bag, or droplet disruption or flame extinction occurred.

One of the video cameras on the rig was used to provide a close-up view of the droplet—this view was backlit. The other video camera, which was orthogonal to the droplet-view camera and was not backlit, provided images of the flame. Both cameras operated at 30 Hz, and images from the cameras were transferred to two SVHS video recorders via fiber optic cables. Representative images from the flame and droplet views are

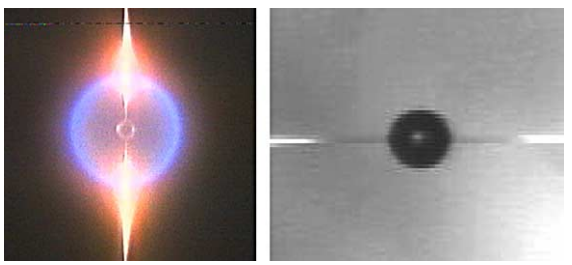

Fig. 2. Representative flame-view and droplet-view images from the experiments.

shown in Fig. 2. The flame-view camera shows some blooming as a result of bright glowing from the portion of the fiber exposed to hot gases from the flame. The blooming occurred because the camera aperture was opened up wide enough to ensure that the blue flame, which emitted visible radiation much more weakly than the fiber, was visible. Clear imaging of the blue flame was necessary so that accurate flame size data could be obtained.

3. Data analysis methods

Flame-view and droplet-view data were analyzed using a Matrox frame grabber and Matrox Inspector software. Flame sizes were measured frame-by-frame by manually drawing a straight line (using the Matrox Inspector software) through the center of the droplet. The diameter of the circular blue flame zone was determined by counting pixels along the line and using the deployment needle size as a size reference. Droplet sizes were measured by a pixel counting computer routine developed at NASA Glenn [16]. The results from both the droplet view and the flame view were synchronized using events that were present in the flame view as well as the droplet view (e.g., deployment needle movements, droplet disruptions (when present), or when the backlight turned off). Uncertainties in size measurements are estimated to be of the order of ±5% to ±10%.

4. Experimental results

The droplets burned in these experiments were readily formed, deployed, and ignited. Light sooting was sometimes observed as yellow coloration evident in the flame views. The flames were very spherical, indicating that buoyancy effects were small. After ignition, the flames rapidly grew in size then leveled off or decreased in size. Droplets generally decreased in size after ignition until flame contractions occurred (for $Y = 0.05$ and 0.2) or the test ended because of the limited time in reduced gravity (for $Y = 0$). Flame contraction was readily evident in the videos as a sudden reduction in the flame radius. In some experiments, the flame extinguished after flame contraction. In others, the droplets experienced disruption (droplet shattering from internal bubble formation and growth) after flame contraction. The random appearance of extinguishment was probably related to small differences between experiments. This would indicate that these droplets were generally close to extinction during flame contraction. The closeness to extinction was likely caused by the high boiling point of glycerol (i.e., droplets must heat substantially during a flame contraction). In the early stages of flame contraction and before substantial droplet heating has occurred, the gas-phase mass fractions of glycerol and propanol may be very low, which would promote extinction.

As a propanol–glycerol droplet burns, propanol will initially be preferentially vaporized from the droplet surface. Because characteristic liquid mass diffusion times are long relative to droplet lifetimes, chemical stratification will occur within a droplet in that a glycerol-rich layer will build at the droplet surface. Since liquid-phase Lewis numbers are larger than unity, heat will diffuse into the droplet interior more efficiently than mass, which can raise the temperature of the propanol-rich droplet interior above a nucleation temperature, which then leads to droplet disruption. The likelihood of droplet disruption is greatest during and after flame contraction because of the rapid increases in droplet surface temperatures that occur during flame contraction events. Microexplosions were likely not observed in some of the present experiments because these droplet extinguished before disruption could occur. It is also noted that Lage et al. [17] have suggested that radiant heat absorption by droplets can influence droplet disruption characteristics, though radiant heat transfer is not expected to be a factor in the present experiments because of the lack of sooting and also since droplets were not burned in hot environments.

Figs. 3 and 4 show representative size histories for droplets and flames with initial glycerol mass fractions of 0.05 and 0.2, respectively. The initial droplet diameter is 0.99 mm for the $Y = 0.05$ mixture and 0.96 mm for the $Y = 0.2$ mixture. Because these experiments employed video cameras, the temporal resolution of the image data was limited to video framing rates (30 Hz), and Figs. 3 and 4 include all of the data points that could be obtained from the videos. Flame size data are not shown in Figs. 3 and 4 at early times because radiant emissions from the igniter wires (before retraction) were bright enough to saturate the video camera, making it difficult to image flames. Distinguishable blue flames appear a few frames after ignition, and flame contractions were clearly evident in the experiment video records at later times. Flame contractions actually take a finite time to occur, and the lines in Figs. 3 and 4 denote the time period from the beginning of the flame contraction to when the flame reaches its minimum size. These figures also show numerical predictions of flame sizes (the solid lines), which will be discussed later.

Figs. 3 and 4 also show experimental results for droplet size variations, with numerical results also shown as the solid lines. The droplet size data in Fig. 3 were extrapolated to the onset of the flame contraction—this extrapolation was necessary as the droplet was not visible for a short time period because the

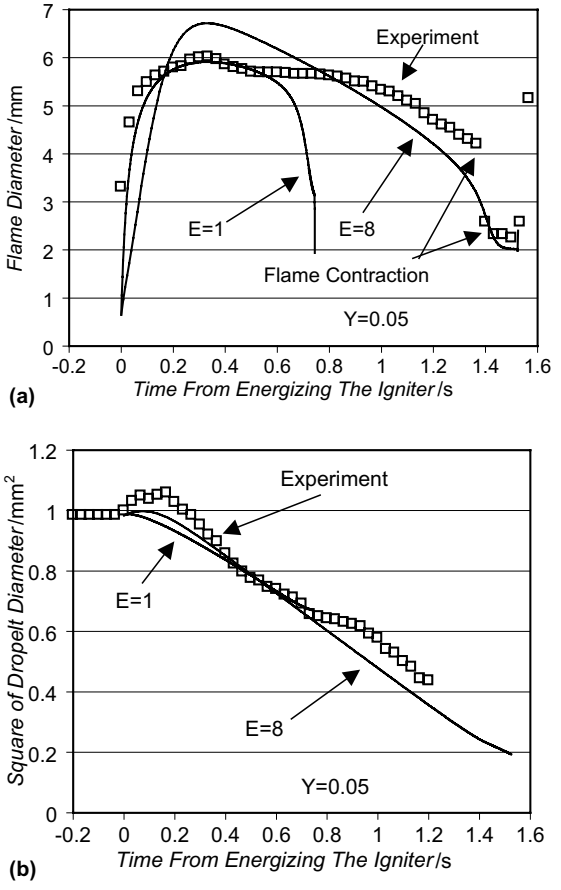

Fig. 3. Histories for (a) flame and (b) droplet sizes ($Y = 0.05$). The symbols are from the experiments and the lines are from the computational model.

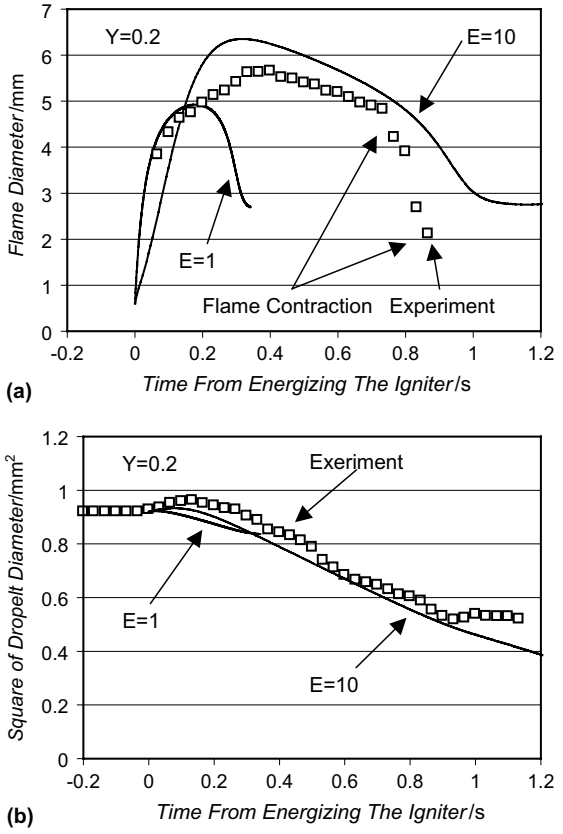

Fig. 4. Histories for (a) flame and (b) droplet sizes ($Y = 0.2$). The symbols are from the experiments and the lines are from the computational model.

backlight turned off early in this particular experiment. The droplet diameter data in Fig. 3 indicate that the d-square law, i.e., where the square of the droplet diameter decreases linearly with time, is basically followed. The same trends are evident in Fig. 4, though the droplet diameter becomes essentially constant after the onset of the flame contraction, and in this particular experiment, the flame extinguished at about 0.74 s after ignition. For the droplet in Fig. 3, a microexplosion occurred at about 1.4 s after the hot wire was energized, terminating the experiment. Prior to the microexplosion and after the flame contraction, it is likely that droplet diameter changes were negligible for the droplet in Fig. 3.

Experimental flame standoff ratios (i.e., instantaneous ratios of flame and droplet diameters) are shown in Fig. 5 for times prior to flame contraction and after early ignition transients have decayed. Flame standoff ratios were nearly constant with values of about 5, indicating that the region between the droplet and the flame was essentially quasisteady. Methanol droplets

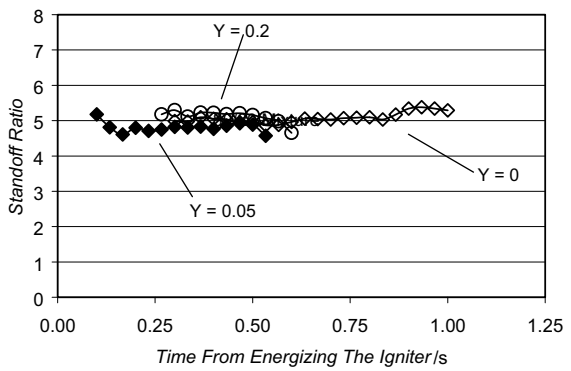

Fig. 5. Ratios of flame and droplet diameters (standoff ratios) obtained from the experiments.

burning in air exhibit quasisteady flame standoff ratios of about 4 [18], while combustion of heptane droplets in air produces unsteady flame standoff ratios that vary

over the range 7–10 [19]. The flame standoff ratios observed for propanol/glycerol droplets lie between those for heptane and methanol droplets, which is reasonable considering the relative amounts of oxygen present in these liquid fuels. In making this statement it is reasonably assumed that vaporization of glycerol was negligible prior to flame contraction.

As noted elsewhere [3], flame contraction data can be used in conjunction with asymptotic theory to estimate effective liquid species coefficients (D) that apply to bicomponent droplet combustion experiments. The values of D calculated to apply to the present experiments using asymptotic theory [3] were $D = 7.3 \times 10^{-9}$ m^2/s for $Y = 0.05$ and $D = 10.1 \times 10^{-9}$ m^2/s for $Y = 0.2$, where uncertainties in the effective diffusivity values are estimated to be about a factor of 2. For comparison, molecular species diffusivities were also calculated. The infinite-dilution diffusion coefficients D°_{ab} and D°_{ba} for glycerol (solute) diffusing into propanol (solvent) and for propanol (solute) diffusing into glycerol (solvent) were calculated using the Tyn–Calus method [20], where the subscripts "a" and "b" denote glycerol and propanol, respectively. Actual species diffusivities, denoted as D_{act}, are expected to be within these limits depending on the liquid composition (it is noted that for highly non-ideal mixtures, species diffusivites can be outside the infinite-dilution limits). It was found that $D^{\circ}_{ab} = 3.06 \times 10^{-9}$ m^2/s and $D^{\circ}_{ba} = 0.123 \times 10^{-9}$ m^2/s when the calculations are performed for the boiling point of propanol (370.5 K). However, since droplets should slowly heat up prior to the onset of flame contraction (from surface buildup of the low-volatility species), calculations were also performed at higher temperatures. For example, a temperature of 475 K, which is an asymptotic estimate for the effective droplet temperature just prior to flame contraction [2,3] yielded the values $D^{\circ}_{ab} = 13.5 \times 10^{-9}$ m^2/s and $D^{\circ}_{ba} = 2.17 \times 10^{-9}$ m^2/s.

The effective D values are about midway between the D°_{ab} and D°_{ba} values calculated for a droplet temperature of 475 K, which is not unreasonable. It is to be noted, however, that the D°_{ab} and D°_{ba} values generally differ by about a factor of 10 for propanol–glycerol mixtures and D_{act} could fall anywhere in the range between D°_{ab} and D°_{ba}, depending on the liquid composition (which can vary appreciably within a droplet when species gradients are present). Considering the wide differences between D°_{ab} and D°_{ba} as well as the uncertainty in the effective diffusivity values, it is not clear from the asymptotic analyses whether D is significantly different from D_{act}. Because of this, a computational model was developed to predict droplet combustion behaviors, with a specific goal of evaluating non-linear variations in liquid species diffusivities in conjunction with spatial and temporal variations in liquid temperature and composition. This computational model is described next.

5. The computational model

The computational model was developed to predict unsteady heat and mass transfer variations in the liquid phase. The model does not currently predict the occurrence of droplet microexplosion or flame extinction, though these phenomena could be modeled by adding the appropriate submodels to the code. In the model, unsteady liquid phase heat and mass transport were assumed to be governed by the following transport equations (where spherical symmetry is assumed). It is noted that T represents temperature and y represents the mass fraction of glycerol.

$$\rho c \frac{\partial T}{\partial t} + \rho c v \frac{\partial T}{\partial r} = \frac{1}{r^2} \frac{\partial}{\partial r} \left(r^2 \lambda \frac{\partial T}{\partial r} \right) \tag{1}$$

$$\frac{\partial y}{\partial t} + v \frac{\partial y}{\partial r} + \frac{1}{\rho} \frac{1}{r^2} \frac{\partial}{\partial r} (r^2 \rho y V) = 0 \tag{2}$$

The variable v appearing in Eqs. (1) and (2) is the bulk liquid velocity while V is the glycerol diffusion velocity. The velocity v in the model is the velocity in the liquid caused by changes in liquid density. This velocity is purely radial and is evaluated using mass conservation, i.e., the liquid-phase momentum equation is not solved. The differential equation for mass conservation (Eq. (3)) is used for evaluation of v.

$$\frac{\partial \rho}{\partial t} + \frac{1}{r^2} \frac{\partial}{\partial r} (r^2 \rho v) = 0 \tag{3}$$

The diffusion velocity V is modeled using Fick's law in the form shown below.

$$yV = -D \frac{\partial y}{\partial r} \tag{4}$$

The use of a spherically symmetrical model is arguably the most straightforward way to investigate whether circulation was significant in the present experiments. This type of approach, which has also been employed for analyses of water absorption during combustion of methanol droplets in reduced gravity [21], provides information on effective diffusivities, which are of interest for engineering calculations [22]. Explicitly putting circulation into the model would require a multidimensional droplet combustion model that involves solving the Navier–Stokes equations both inside and outside the droplet while accounting for the presence of the fiber and the initial conditions associated with droplet formation, deployment and ignition. This type of model would be prohibitively difficult to develop and is a major research project in itself. It is also noted that a such multidimensional model would require information on the initial droplet interior flowfield, and this information was not available.

Introducing the variable $z = r/R$ transforms Eqs. (1) and (2) to the following forms.

$$\frac{\partial T}{\partial t} = \frac{\lambda}{R^2\rho c}\frac{\partial^2 T}{\partial z^2} + \frac{1}{R^2\rho c}\left(\frac{\partial \lambda}{\partial z} + \frac{2\lambda}{z} + \rho c R\dot{R}z - \rho c R v\right)\frac{\partial T}{\partial z} \tag{5}$$

$$\frac{\partial y}{\partial t} = \frac{D}{R^2}\frac{\partial^2 T}{\partial z^2} + \left[\frac{\partial D}{\partial z} + D\left(\frac{2}{z} + \frac{1}{\rho}\frac{\partial \rho}{\partial z}\right) + R\dot{R}z - Rv\right]\frac{\partial y}{\partial z} \tag{6}$$

Spatial variations in the properties ρ, λ and D are accounted for in this model through the terms $\partial\rho/\partial z$, $\partial\lambda/\partial z$ and $\partial D/\partial z$. In addition, as noted previously, all liquid properties were allowed to vary spatially and temporally.

The liquid-phase radial velocity at any radius r can be related to the time-rate-of-change of the liquid density by integrating Eq. (3), as shown in Eq. (7).

$$v = -\frac{1}{\rho r^2}\int_0^r r^2\frac{\partial \rho}{\partial t}\,\mathrm{d}r \tag{7}$$

Using the variable $z = r/R$ allows Eq. (7) to be expressed as follows:

$$v = -\frac{1}{\rho R z^2}\int_0^z \left(R\frac{\partial \rho}{\partial t} + 3\dot{R}\rho\right)z^2\,\mathrm{d}z + \dot{R}z \tag{8}$$

The boundary conditions at the droplet center are as follows:

$$\left(\frac{\partial T}{\partial z}\right)_{z=0} = \left(\frac{\partial y}{\partial z}\right)_{z=0} = 0 \tag{9}$$

In addition, the calculations employed the initial conditions $T(z,0) = 298$ K and $y(z,0) = Y$.

At the droplet surface ($z = 1$) boundary conditions to enforce conservation of mass, species and energy were applied. In particular, the following boundary conditions were used for conservation of energy and species, where the subscripts + and − denote the gas and liquid sides of the gas–liquid interface, respectively.

$$\left(\frac{\partial T}{\partial z}\right)_- = \frac{\lambda_+}{\lambda_-}\left(\frac{\partial T}{\partial z}\right)_+ - \frac{\dot{m}L}{4\pi R^2\lambda_-} \tag{10}$$

$$\left(\frac{\partial y}{\partial z}\right)_- = \frac{Rv_- - R\dot{R}}{D_-}y_- - \frac{R\rho_+ v_+}{\rho_- D_-}\delta \tag{11}$$

The variable δ appearing in Eq. (11) is the mass-flux fraction of glycerol leaving the droplet, i.e., δ is the ratio of the glycerol mass flow rate from the droplet surface to the total mass flow rate $\dot{m}$. The heat of vaporization L appearing in Eq. (10) is given by $L = \delta L_a + (1-\delta)L_b$, where L_a and L_b are the enthalpies of vaporization of glycerol and propanol, respectively (it is noted that the computations showed that glycerol vaporization was negligible, i.e., $\delta \ll 1$, prior to flame contraction). Eq. (11) was derived assuming that the droplet surface regression rate is small relative to gas-phase velocities at the droplet–gas interface, which is reasonable considering the large density differences that exist between the liquid and gas phases for the subcritical pressures considered here.

To employ these boundary conditions, expressions are needed for the terms that apply to the gas side of the gas–liquid interface, i.e., ρ_+, v_+, $(\partial T/\partial r)_+$ and δ. In this analysis, it is assumed that the gas phase can be treated as quasisteady, allowing analytical results for conservation of mass, energy and species to be used for the gas phase. This type of approach has also been employed by other researchers [17]. The assumption of a quasisteady gas phase is justified from the experimental results. For example, Fig. 5 shows that flame standoff ratios were steady, indicating quasisteady conditions between the droplet and the flame. It will also be shown later that use of a quasisteady gas phase assumption leads to reasonable agreement between the numerical and experimental results for flame behaviors.

The analytical gas-phase results used here were obtained from [23,24] and are not repeated here for brevity. It is noted that combustion is allowed for in these calculations in the sense that a one-step overall reaction is assumed. Average gas-phase properties were evaluated using results from the literature [20,25–27]. The results from [23] assume that the Lewis number for the gas phase has a value of unity. While this assumption can produce reasonable results for burning rates, flame standoff ratios are generally predicted to be too large using a Lewis number of unity. Because of this, the approximate theory developed in [24] for predicting quasisteady flame standoff ratios while allowing for distinct binary species diffusion coefficients was used (i.e., no assumptions about the gas-phase Lewis number were invoked). As shown below, this theory provides reasonable agreement between the experiments and the numerical calculations in terms of flame standoff ratios.

It is noted that inclusion of the liquid-phase velocity field in the species and energy transport equations required also that v be accounted for when calculating values of $R\dot{R}$. This was accomplished by applying of mass conservation principles, yielding Eq. (12) below.

$$R\dot{R} = Rv_- - \frac{\dot{m}}{4\pi R\rho_-} \tag{12}$$

The first term in Eq. (12) accounts for droplet swelling while the second term accounts for mass loss from the droplet surface. Examination of Eq. (12) shows that conditions can exist where $R\dot{R} > 0$, leading to increases in the droplet radius with time as a result of decreases in liquid density. As described later, calculations predict

the occurrence of droplet swelling at early times, which is in accordance with the experimental results.

An implicit finite difference code was written to simultaneously solve the liquid-phase conservation equations for the temperature and mass fraction profiles within a droplet. The numerical scheme used a Crank-Nicholson method for the integration of Eqs. (5) and (6); this scheme employed second order accurate approximations for spatial derivatives. Eq. (8) was evaluated at each time step by evaluating $\partial\rho/\partial t$ with a first-order backward difference formulation and then integrating spatially by using the trapezoidal rule. The boundary conditions were evaluated using second order difference equations. Because the resulting difference equations were not tridiagonal, a special routine was developed to transform the difference equations to a tridiagonal form at each time step, after which they were solved using a tridiagonal solver.

All liquid properties were evaluated at each grid point and time (i.e., liquid properties vary with respect to temperature and composition, which in turn, are dependent on space and time). Liquid properties were evaluated using established correlations for pure liquids and liquid mixtures [20,26,27]. For example, liquid activity coefficients were calculated using a subroutine that was based on the UNIFAC method [20]. These activity coefficients were used for prediction of vapor pressures as well as non-ideal liquid effects on liquid species diffusion rates [20].

It is mentioned that during the code development, a general-purpose code was first written to solve the generic diffusion equation shown below in Eq. (13). This equation is of the same general form as Eqs. (5) and (6).

$$\frac{\partial\phi}{\partial t} = a_1\frac{\partial^2\phi}{\partial z^2} + a_2\frac{\partial\phi}{\partial z} \tag{13}$$

This generic code, which employed the numerical schemes mentioned above, was written so that the coefficients a_1 and a_2 in Eq. (13) were allowed to vary temporally and spatially as the solution progressed. This code was tested using various boundary conditions and initial conditions by comparison with exact analytical solutions that are known for different situations (e.g., transient heat transfer in a sphere). Once the code was verified to provide accurate solutions for these cases, the coefficients a_1 and a_2 were rewritten to allow solutions of Eqs. (5) and (6) to be developed (where ϕ was replaced with T and y).

Calculations were performed using two different types of spatial grids, uniform and non-uniform. The non-uniform grids were generated using Eq. (14).

$$z(i) = 1 + \beta\ln\left[1 - (1 - e^{-1/\beta})\frac{N-i}{N-1}\right] \tag{14}$$

In Eq. (14), $z(i)$ is the spatial location of the ith grid point, β is a grid spacing parameter, and N is the total number of grid points. Reducing β clusters more grid points near the droplet surface. For example, for the non-uniform grid, using $\beta = 0.3$ with 201 nodes gave results that closely matched a 1001 node uniform grid scheme. The conversion to the non-uniform grid scheme could reduce computing times by a factor of about 6. The non-uniform grid worked well for this problem because sharp gradient regions appeared near the liquid side of the gas–liquid interface, which was where the grid was finest. Convergence was checked by varying time steps and grid spacings until grid-independent and time step-independent results were obtained for both types of grids. It is noted that property value calculations lagged one time step behind the T and y calculations. However, because property values did not change rapidly in time, this lag did not introduce significant errors into the results. Furthermore, the time steps were sufficiently small to ensure time step independent results.

Finally, it is noted that calculations were also performed to estimate the amount of water that might be absorbed into the liquid phase of a propanol–glycerol droplet. It was found that maximum local water mass fractions were of the order of 1% or less because of non-ideal mixture effects (i.e., water activity coefficients were generally larger than unity) as well as the relatively high boiling points of propanol and glycerol. As a result, water absorption effects are neglected in all of the calculations presented here.

6. Computational results

Figs. 6 and 7 present results from the numerical model regarding transient variations in the liquid surface mass fraction of glycerol as well as the droplet surface temperature, respectively. It should be noted that the calculations became very stiff as the surface mass fraction of glycerol, denoted as y_{-}, closely approached unity.

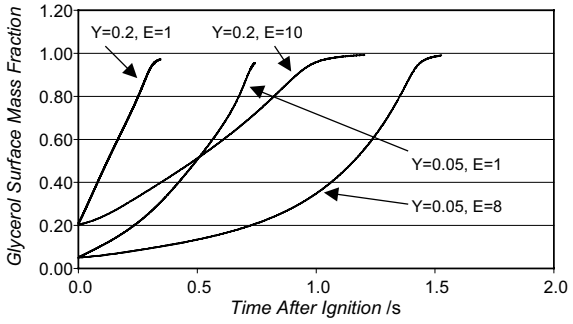

Fig. 6. Glycerol surface mass fraction profiles predicted by the numerical model.

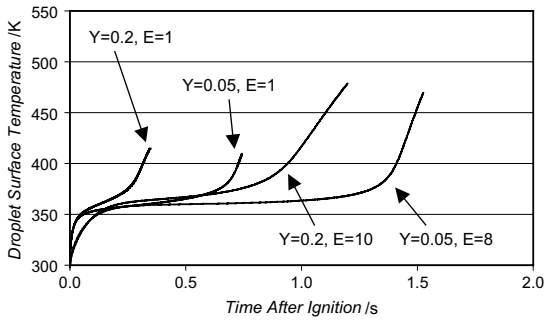

Fig. 7. Droplet surface temperature profiles predicted by the numerical model.

The calculations were typically stopped when y_- exceeded about 0.98, which corresponded to estimates made using available asymptotic theory for a flame contraction to occur [3]. It is also noted that in Figs. 3 and 4, the computational flame histories show reductions in flame sizes as y_- approached unity closely, which is consistent with asymptotic theory [3].

The calculations in Figs. 6 and 7 correspond to cases where the liquid thermal conductivity and species diffusivity were enhanced by various factors. In these figures, the variable E represents the factor by which the molecular transport properties λ and D were increased everywhere within the droplet (the same E values were applied to both λ and D for a given calculation). As shown in Fig. 6, y_- initially builds rapidly and then increases more slowly as a value of unity is approached. As would be expected, the approach to unity occurs much sooner for $Y = 0.2$ than for $Y = 0.05$ (it should also be noted that the calculations were performed for the same initial droplet diameters as for the experiments). In addition, increasing E (the liquid transport enhancement factor) increases the time required for y_- to approach unity.

These trends are also consistent with the droplet surface temperature profiles shown in Fig. 7. In general, droplet surface temperature profiles show an initial heatup period that occurs shortly after ignition. Following this, droplet surface temperatures rise slowly as the surface mass fraction of glycerol builds up; the droplet surface temperatures during this time period are in the range of the saturation temperature of the more volatile component (propanol). As y_- approaches unity, droplet surface temperatures begin to increase sharply as the flame contraction commences. Increasing E increases the time period before strong temperature variations occur at the onset of flame contraction.

Figs. 3 and 4 show experimental results for droplet size variations, with the numerical results superimposed as the solid lines. A good match between experimental and theoretical results on burning rates was needed to effectively compare the onset of flame contraction predicted by the model with experimental results (see below). The computational model assumes that the gas phase between the droplet and the flame has a constant thermal conductivity, and this thermal conductivity was adjusted from what is recommended for combustion of fuel droplets in air [28] in order to improve agreement between theory and experiment on burning rates.

Initial droplet swelling from droplet density increases is evident in both the computational and experimental results in Figs. 3 and 4. The swelling in the experiments was slightly larger than predicted by the computations, though the swelling predicted by the computational model is essentially within the uncertainty of the experimental measurements.

Figs. 3 and 4 also show experimental flame size data as well as computational predictions of flame sizes. Consistent with the experiments, comparison of Figs. (3) and (4) shows that flame contraction occurs more sharply when the initial mass fraction of glycerol is decreased. As shown in Figs. 3 and 4, the numerical simulations predict that the onset of flame contraction occurs much earlier than it occurred in the experiments when the value $E = 1$ was used, which suggests that liquid-phase convective mixing may have been present in the droplets. In general, agreement between experiments and computations for flame diameters was reasonable, indicating that the assumption of a quasisteady gas phase is acceptable.

The calculations indicate that the liquid species diffusivity and thermal conductivity values used in the numerical model should be increased by factors between about 8 and 10 for the numerical flame contraction times to match the experimental flame contraction times (see the $E = 8$ and 10 calculations in Figs. 3 and 4). It is noted that applicable effective diffusivities were determined by repeatedly running the computer code and then directly comparing droplet and flame data from the experiments with the computational results. These data comparisons were performed manually. These increases are larger that what would be considered to apply to droplets with Hills-type vortex flows inside droplets [5], suggesting that the flows in the droplets had smaller diffusive length scales than would be expected from a single Hills vortex. As a result, the droplets may have contained more than one vortex or perhaps chaotic flows may have been present in these droplets, which can cause larger increases in effective diffusivities [6]. These types of flows are consistent with experimental observations of flow patterns inside droplets burning in microgravity environments [29], where random flows were observed using flow visualization techniques.

Droplet internal circulation could have resulted from droplet formation and deployment processes. Because of the limited reduced-gravity time available in an

experiment, internal circulation of this type may not have had sufficient time to damp to negligible levels prior to ignition. To show this, we consider a characteristic time for viscous decay of droplet internal flows, estimated as d^2/v, where v is a characteristic liquid kinematic viscosity. For the present experiments, $d \approx 10^{-3}$ m and $v \approx 10^{-6}$ m^2/s (prior to ignition), yielding $d^2/v \approx 1$ s. For droplet internal flows to decay to negligible levels, ignition would need to be delayed (after needle retraction) for times somewhat larger than d^2/v, which could not be achieved in the present experiments. It is also noted that because of the large differences in surface tension between glycerol and propanol, mixing driven by Marangoni flows may have also played a role. However, without information on the character of the flowfields within the droplets, it is difficult to precisely determine the cause(s) of any circulation.

It is noted that the hardware used in the present experiments is of a type that is commonly employed in reduced-gravity droplet combustion experiments. As a result, the results described here are of interest to other workers in this area. For example, the results in the paper indicate that significant mixing was present in these experiments, showing that special hardware considerations will be required if internal liquid circulation is to be suppressed. It would also be useful to perform further research to determine the source(s) of droplet internal convection. In this way, new experiments might be designed that would allow control (and characterization) of internal liquid circulation so that convective influences on droplet behaviors could be experimentally determined.

7. Conclusions

This research has demonstrated that reduced-gravity experiments on combustion of propanol–glycerol droplets are readily performed. The experiments demonstrated relatively clean burning (i.e., little soot) with easily observable flame contractions. In addition, it was observed that flame standoff ratios were essentially steady with values of about 5 (prior to flame contraction and after initial ignition transients have decayed). The occurrence of flame extinction was sometimes observed following flame contraction. The appearance of extinction, which appeared to be random, was probably related to small differences between experiments, indicating that these droplets were generally close to extinction during flame contraction. In the early stages of flame contraction and before substantial droplet heating has occurred, the gas-phase mass fractions of propanol and glycerol may be very low, which would promote extinction.

Experimental data for the onset of flame contraction were used with an asymptotic model to estimate effective liquid species diffusivities that were applicable to these experiments. It was found, however, that infinite-dilution liquid species diffusion coefficients could differ by about a factor of 10 for propanol–glycerol mixture droplets, which made it difficult to determine whether significant convective mixing was present in the droplets by simply comparing effective species diffusivities with infinite-dilution species diffusivities.

Transient numerical simulations provided better indications as to the likelihood that convective mixing was occurring in the droplets. The numerical model included variable liquid transport properties as well as non-linear variations in liquid species diffusion coefficients. Comparison of experimental results on onset times for flame contraction with results from the numerical model suggest that liquid species diffusivity values used in the numerical model should be increased by factors between about 8 and 10 for the numerical flame contraction times to match the experimental flame contraction times. These increases are larger that what would be considered to apply to droplets with Hills-type vortex flows inside droplets [5], suggesting that the flows in the droplets had smaller diffusive length scales than would be expected from a single Hills vortex. As a result, the droplets may have contained more than one vortex or perhaps chaotic flows may have been present in these droplets, which can cause larger increases in effective diffusivities [6]. These types of flows are consistent with experimental observations of flow patterns inside droplets burning in microgravity environments [29], where random flows were observed using flow visualization techniques.

It is of interest to extend this research. For example, the numerical model could be extended to include adaptive gridding and adaptive timestep control. The assumption of a quasisteady gas phase could be relaxed, with the inclusion of finite-rate chemical kinetics to allow prediction of extinction (which was observed in the experiments) as well as variable properties in the gas phase. It is also of interest to perform further experiments with other droplet compositions and other ambient environments. In addition, flow visualization experiments would allow characterization of droplet internal flow fields, providing important information on how the droplet internal flowfield influences effective species diffusion coefficients within droplets.

Acknowledgements

The research presented here has been performed in support of a NASA-sponsored program to investigate the effects of droplet internal flows on combustion behaviors of fuel droplets under reduced-gravity conditions. This experiment program is termed the Bi-Com-

ponent Droplet Combustion Experiment (BCDCE). The support of the NASA Microgravity Combustion Program is gratefully acknowledged. The Technical Monitor for this research was Doctor Daniel L. Dietrich. Brian Borowski and his staff are gratefully acknowledged. The efforts of Miguel Perez and Dr. Jingbin Wei in supporting this research are gratefully acknowledged. The authors would also like to thank Peter Struk and all the technicians including Joe Carrion, Chris Hampton, and Mark McMillan at the 2.2 s drop tower for their assistance.

References

[1] C.H. Wang, X.Q. Liu, C.K. Law, Combustion and microexplosion of freely falling multicomponent droplets, Combustion and Flame 56 (1984) 175–197.

[2] B.D. Shaw, F.A. Williams, Theory of influence of a low-volatility, soluble impurity on spherically symmetric combustion of fuel droplets, International Journal of Heat and Mass Transfer 33 (1990) 301–317.

[3] I. Aharon, B.D. Shaw, Estimates of liquid species diffusivities from experiments on reduced-gravity combustion of heptane–hexadecane droplets, Combustion and Flame 113 (1998) 507–518.

[4] I. Aharon, B.D. Shaw, Marangoni instability of bicomponent droplet gasification, Physics of Fluids 8 (1996) 1820–1827.

[5] J.-P. Delplanque, R.H. Rangel, W.A. Sirignano, Liquid-waste incineration in a parallel-stream configuration: effect of auxiliary fuel, in: Progress in Astronautics and Aeronautics, 132, AIAA, Washington, DC, 1991, pp. 164–186.

[6] M.D. Bryden, H. Brenner, Mass-transfer enhancement via chaotic laminar flow within a droplet, Journal of Fluid Mechanics 379 (1999) 319–331.

[7] B.D. Shaw, B.D. Clark, D.F. Wang, Spacelab experiments on combustion of heptane–hexadecane droplets, AIAA Journal 39 (2001) 2327–2335.

[8] D.L. Dietrich, J.B. Haggard Jr., F.L. Dryer, V. Nayagam, B.D. Shaw, F.A. Williams, Droplet combustion experiments in Spacelab, in: Twenty-Sixth International Symposium on Combustion, The Combustion Institute, Pittsburgh, 1996, pp. 1201–1207.

[9] J.C. Yang, C.T. Avedisian, Combustion of unsupported heptane–hexadecane mixture droplets at low gravity, in: Twenty-Second Symposium (International) on Combustion, The Combustion Institute, Pittsburgh, 1988, pp. 2037–2044.

[10] J.C. Yang, G.S. Jackson, C.T. Avedisian, Combustion of unsupported methanol/dodecanol mixture droplets at low gravity, in: Twenty-Third Symposium (International) on Combustion, The Combustion Institute, Pittsburgh, PA, 1990, pp. 1619–1625.

[11] B.D. Shaw, I. Aharon, D. Lenhart, D.L. Dietrich, F.A. Williams, Spacelab and drop tower experiments on reduced gravity combustion of methanol/dodecanol and ethanol/dodecanol mixture droplets, Combustion Science and Technology 167 (2001) 29–56.

[12] K. Okai, O. Moriue, M. Araki, M. Tsue, M. Kono, J. Sato, D.L. Dietrich, F.A. Williams, Pressure effects on combustion of methanol and methanol/dodecanol single droplets and droplet pairs in microgravity, Combustion and Flame 121 (2000) 501–512.

[13] G.S. Jackson, C.T. Avedisian, J.C. Yang, Observations of soot during droplet combustion at low gravity: heptane and heptane/monochloroalkane mixtures, International Journal of Heat and Mass Transfer 35 (1992) 2017–2033.

[14] M.Y. Choi, F.L. Dryer, Microgravity droplet combustion, in: H.D. Ross (Ed.), Microgravity Combustion: Fire in Free Fall, Academic Press, New York, 2001, pp. 183–297.

[15] J. Lekan, Microgravity research in NASA ground-based facilities, NASA TM-101397 1989.

[16] P.M. Struk, M. Ackerman, V. Nayagam, D.L. Dietrich, On calculating burning rates during fiber supported droplet combustion, Microgravity Science and Technology XI/4 (1998) 144–151.

[17] P.L.C. Lage, C.M. Hackenberg, R.H. Rangel, Nonideal vaporization of dilating binary droplets with radiation absorption, Combustion and Flame 101 (1995) 36–44.

[18] A.J. Marchese, F.L. Dryer, R.O. Colantonio, V. Nayagam, Microgravity combustion of methanol and methanol/water droplets: drop tower experiments and model predictions, in: Twenty-Sixth Symposium (International) on Combustion, The Combustion Institute, Pittsburgh, PA, 1996, pp. 1209–1217.

[19] A.J. Marchese, F.L. Dryer, V. Nayagam, Numerical modeling of isolated *n*-alkane droplet flames: initial comparisons with ground and space-based microgravity experiments, Combustion and Flame 116 (1998) 432–459.

[20] R.C. Reid, J.M. Prausnitz, B.E. Poling, The Properties of Gases and Liquids, fourth ed., McGraw-Hill, New York, 1987.

[21] A.J. Marchese, F.L. Dryer, The effect of liquid mass transport on the combustion and extinction of bicomponent droplets of methanol and water, Combustion and Flame 105 (1996) 104–122.

[22] W.A. Sirignano, Fluid Dynamics and Transport of Droplets and Sprays, Cambridge University Press, Cambridge, UK, 1999.

[23] B.D. Shaw, Studies of influences of liquid-phase species diffusion on spherically symmetric combustion of miscible binary droplets, Combustion and Flame 81 (1990) 277–288.

[24] I. Aharon, B.D. Shaw, On the roles of thermal diffusion and distinct binary diffusion coefficients in modeling droplet flame locations in microgravity, Microgravity Science and Technology X/2 (1997) 75–85.

[25] S.I. Sandler, Chemical and Engineering Thermodynamics, second ed., John Wiley and Sons, New York, 1989.

[26] R.H. Perry, Perry's Chemical Engineers' Handbook, seventh ed., McGraw-Hill, New York, 1997.

[27] C.L. Yaws, Chemical Properties Handbook, McGraw-Hill, New York, 1999.

[28] F.A. Williams, Combustion Theory, second ed., Benjamin Cummings, Menlo Park, CA, 1984.

[29] B.D. Shaw, A.G. Chen, Observation of flows inside droplets undergoing combustion in reduced gravity, Microgravity Science and Technology X/3 (1997) 136–143.